Available online at www.sciencedirect.com
SCIENCE DIRECT®
Catalysis Today 96 (2004) 11–20
CATALYSIS TODAY
www.elsevier.com/locate/cattod

Support and particle size effects on direct NO decomposition over platinum

Xianqin Wang, Susan M. Sigmon, James J. Spivey[1], H. Henry Lamb*

Department of Chemical Engineering, North Carolina State University, Raleigh, NC 27695-7905, USA

Available online 24 June 2004

Abstract

Supported Pt catalysts were prepared by ion exchange of Pt(II) tetraamine hydroxide [$Pt(NH_3)_4(OH)_2$] onto SiO_2, Al_2O_3, and TiO_2 and by adsorption of Pt bis-acetylacetonate [$Pt(acac)_2$] onto MgO. All the catalysts except Pt/TiO_2 were characterized by in situ X-ray absorption fine structure (XAFS) spectroscopy after reduction at 300 °C in flowing H_2, and the Pt/SiO_2 and Pt/MgO catalysts were examined after subsequent exposure to 1% NO/He at 25–300 °C. NO decomposition pathways were investigated by temperature-programmed reaction spectroscopy (TPRS) using a 1% NO/He feed, and steady-state conversions for direct NO decomposition were measured at 600 °C. NO decomposition at low temperatures (200–400 °C) produces N_2O and N_2, and in situ XAFS spectroscopy indicates that the supported Pt particles are partially oxidized under these conditions. Over each catalyst, O_2 production begins at ~350 °C; N_2O production declines above 400 °C; and N_2 and O_2 are the only detectable NO decomposition products at 600 °C. Nanometer-sized Pt clusters on SiO_2 sinter during heating in 1% NO/He at 300 °C, whereas larger Pt particles supported on SiO_2 and MgO are resistant to sintering under these conditions. The turnover frequency for direct NO decomposition over Pt/SiO_2 catalysts is insensitive to Pt particle size. Pt/SiO_2, Pt/Al_2O_3, and Pt/TiO_2 catalysts have equivalent NO decomposition activities suggesting the absence of support effects for these metal oxides. In contrast, the NO decomposition activity of Pt supported on strongly basic MgO is significantly lower.

Keywords: NO decomposition; Temperature-programmed reaction spectroscopy; EXAFS spectroscopy; XANES spectroscopy; Support effects; Particle size effects

1. Introduction

More stringent NO_x emission requirements for diesel engines will require catalytic NO_x abatement technologies that are effective under lean-burn conditions. Direct NO decomposition to N_2 and O_2 (without an added reductant) is an attractive alternative to NO_x traps and selective catalytic reduction for this application [1]. NO decomposition is thermodynamically favorable; however, a practical catalyst must exhibit high activity at low temperatures (200–300 °C) in an oxygen-rich environment [2]. Supported Group VIII metals, such as Pt, Pd, Rh, and Ru, exhibit varying degrees of NO decomposition activity albeit at high temperatures (600–800 °C) [3–5]. Pt and Pd are the most active of these metals; however, supported Pt and Pd catalysts deactivate rapidly at low temperatures due to oxygen poisoning [3,6]. At higher temperatures, O_2 desorption has been inferred to be the rate-determining step in catalytic NO decomposition over Pd/Al_2O_3 catalysts [7]. The results of a recent study suggest the same conclusion for Pt/Al_2O_3 catalysts [8]; however, earlier investigations of the kinetics of NO decomposition over supported Pt catalysts and polycrystalline Pt yielded rate expressions consistent with quasi-equilibrated O_2 adsorption [9–11].

NO dissociative chemisorption on Pt surfaces is highly structure sensitive as evidenced by numerous temperature-programmed desorption (TPD) studies conducted on Pt single crystals [4]. Moreover, the catalytic activity of a Pt surface for NO reduction (e.g., the CO–NO reaction) depends on its NO dissociation efficiency. NO dissociation generally is enhanced for Pt surfaces on which the atoms have lower coordination numbers, i.e., more open crystal planes and surfaces with high densities of steps and kinks. For example, NO adsorbs molecularly on Pt(1 1 1); however, a significant portion of adsorbed NO dissociates on Pt(1 0 0) [12]. During TPD the adsorbed nitrogen and oxygen atoms desorb associatively to produce N_2 and O_2, respectively. O_2

* Corresponding author. Tel.: +1 919 515 6395; fax: +1 919 515 3465.
E-mail address: lamb@eos.ncsu.edu (H.H. Lamb).
[1] Present address: Department of Chemical Engineering, Louisiana State University, Baton Rouge, LA, USA.

0920-5861/$ – see front matter © 2004 Elsevier B.V. All rights reserved.
doi:10.1016/j.cattod.2004.05.003

desorption from Pt(1 0 0) has the higher activation barrier as evidenced by the TPD peak temperature (~650 K) [13] consistent with the hypothesis that O_2 desorption is the rate-determining step in direct NO decomposition.

Particle size effects have been studied extensively in supported metal catalysis, especially for hydrocarbon conversion reactions [14]. Studies of model Pd/SiO_2 and Pd/Al_2O_3 catalysts have shown that NO dissociation is more efficient on smaller Pd particles than larger ones, presumably because of the higher percentage of edge and corner sites [15]. We are not aware, however, of a similar study of particle size effects for NO dissociation on supported Pt catalysts. The early work of Boudart and coworkers indicated that direct NO decomposition over Pt is not structure sensitive, since equivalent turnover frequencies (TOFs) were found for Pt/Al_2O_3 catalysts with dispersions of 3.7 and 39% [9,10]. A more recent study verified that particle size effects are small for direct NO decomposition over Pt/Al_2O_3 catalysts [8].

The metal oxide support can influence the catalytic activity of supported Pt in a number of different ways, including effects on particle size, morphology, resistance to sintering, oxidation resistance, and Pt electronic structure. Moreover, the support can be directly involved in the catalysis via spillover (and reverse spillover) of reaction intermediates. We are not aware of an investigation of support effects on Pt-catalyzed NO decomposition since Sakata et al. [16] examined Pt supported on a variety of metal oxides in 1978.

In this work, supported Pt catalysts were prepared by ion exchange of Pt(II) tetraamine hydroxide [$Pt(NH_3)_4(OH)_2$] onto SiO_2, Al_2O_3, and TiO_2 and by adsorption of Pt bis-acetylacetonate [$Pt(acac)_2$] onto MgO. All the catalysts (except Pt/TiO_2) were characterized by in situ X-ray absorption fine structure (XAFS) spectroscopy after reduction at 300 °C in flowing H_2, and the Pt/SiO_2 and Pt/MgO catalysts were examined after subsequent exposure to 1% NO/He at 25–300 °C. Temperature-programmed reaction spectroscopy (TPRS) was used to investigate NO decomposition pathways, and steady-state NO decomposition activities were measured at 600 °C. The results provide new insight into the effects of Pt particle size and the metal oxide support on direct NO decomposition catalysis.

2. Experimental methods

2.1. Catalyst preparation

SiO_2 (Degussa, Aerosil 200), Al_2O_3 (Vista, Catapal A), TiO_2 (Degussa, P25) and MgO (Martin Marietta Magnesia Specialties, Magchem AD) were used as received. Ultra-high-purity He and H_2, extra-dry O_2 and a certified 1% NO/He mixture were supplied by National Welders.

Supported Pt catalysts were prepared by ion exchange of aqueous Pt(II) tetraamine hydroxide with SiO_2, Al_2O_3, and TiO_2. In a typical preparation, an aqueous solution containing $Pt(NH_3)_4(OH)_2$ was added dropwise to a slurry of support (5 g) and deionized (DI) water (50 mL) at 25 °C. After stirring overnight, the solid was recovered by filtration, washed with DI water, and dried at 80 °C overnight. Two Pt/SiO_2 catalysts [designated Pt/SiO_2(1) and Pt/SiO_2(2)] were prepared with different Pt loadings. Pt/SiO_2(1) was calcined in flowing O_2 at 230 °C for 2 h, and the other catalysts were calcined in O_2 at 300 °C.

A Pt/MgO catalyst was prepared by adsorption of $Pt(acac)_2$ onto MgO from toluene solution. MgO powder (180 m^2/g) was pretreated in flowing O_2 at 500 °C for 5 h and transferred to a N_2-filled glovebox without exposure to air. A solution of $Pt(acac)_2$ (Strem Chemicals) in toluene (100 mL) was added to 5 g of pretreated MgO suspended in toluene (10 mL), and the resulting slurry was stirred overnight in the glove box. The light-yellow Pt/MgO catalyst was recovered by filtration and dried for 5 h on a vacuum line.

The supported Pt catalysts were stored in sealed vials in a desiccator. Pt loadings (Table 1) were determined at Galbraith Laboratories by ICP-OES with the exception of the Pt/Al_2O_3 catalyst. The Pt loading of this sample was determined from the Pt L_3 X-ray absorption edge jump using the other catalyst samples as calibration standards.

2.2. X-ray absorption spectroscopy (XAS)

Pt L_3 edge (11564 eV) XA spectra were measured using beam line X-11A of the National Synchrotron Light Source at Brookhaven National Laboratory. The storage ring operated with an electron energy of 2.8 GeV and a current between 150 and 300 mA. The Si(1 1 1) double-crystal X-ray monochromator was calibrated using a 25 μm Pt foil. Measurements were made in transmission mode; the I_0 ionization chamber contained flowing 20% Ar/N_2, and the I chamber contained flowing Ar. The XA spectra were collected in four ranges (−200, −30, 30 eV, and 8, 16 $Å^{-1}$) with step sizes of 10 and 0.5 eV, and 0.07 and 0.07 $Å^{-1}$, respectively. For each sample condition, two or three spectra were recorded and averaged to increase the signal-to-noise ratio. All XA spectra were recorded at 25 °C. We were unable to characterize the Pt/TiO_2 catalyst by transmission Pt L_3 XAS due to the strong X-ray absorption background.

Each sample (with a weight of 0.1–0.2 g) was pressed into a rectangular slot in a stainless steel sample holder which was then mounted in an in situ XAS cell [17]. Each sample was reduced at 300 °C in flowing H_2 for 1 h, purged briefly with He at 300 °C, cooled in flowing He to 25 °C, and sealed under He in the XAS cell. After the initial XAS measurements, the reduced Pt/SiO_2 and Pt/MgO samples were exposed briefly to flowing 1% NO/He at 25 °C, sealed under this mixture, and the XA spectra measured. Selected samples were heated to 300 °C in flowing 1% NO/He, soaked for 30 min at 300 °C, cooled to <50 °C in flowing 1% NO/He, purged with He, and sealed under He in the XAS cell.

The extended X-ray absorption fine structure (EXAFS) spectra were analyzed using XDAP software [18] follow-

Table 1
Summary of NO decomposition activity of supported Pt catalysts

Catalyst	Pt loading (wt.%)	D[a]	Conversion[b,c] (300 °C reduction)	Rate[c,d] (mol NO/mol Pt s)	TOF (s^{-1}) (300 °C reduction)	Conversion[b,e] (500 °C reduction)	Rate[d,e] (mol NO/mol Pt s)
Pt/SiO_2(1)	0.65	0.56	30.0	0.0066	0.0117	–	–
Pt/SiO_2(2)	1.89	0.38	42.1	0.0035	0.0091	44.1	0.0037
Pt/Al_2O_3	0.62	–	26.6	0.0060	–	17.2	0.0036
Pt/TiO_2	0.75	–	19.6	0.0035	–	19.1	0.0034
Pt/MgO[f]	0.78	–	8.9	0.0014	–	12.4	0.0020

[a] Pt dispersion estimated using Pt–Pt coordination number measured by in situ EXAFS after NO treatment at 300 °C.
[b] Steady-state NO conversion for a 1% NO/He feed at 600 °C.
[c] Catalysts were reduced in situ at 300 °C in H_2 prior to testing.
[d] Rate extrapolated to 0% conversion for a 1% NO/He feed.
[e] Catalysts were reduced in situ at 500 °C in H_2 prior to testing.
[f] Catalyst derived from $[Pt(acac)_2]$ precursor.

ing procedures described in more detail elsewhere [19]. The EXAFS spectrum was isolated from the XAS data and normalized using the height of the edge jump at 50 eV. The resulting χ data were fitted in R space yielding the EXAFS structural parameters: N (coordination number), R (interatomic distance), $\Delta\sigma^2$ (relative Debye–Waller factor), and ΔE_0 (inner potential shift). Reference files were derived from the EXAFS spectrum of Pt foil measured at 25 °C and $[Na_2Pt(OH)_6]$ measured at liquid-nitrogen temperature.

2.3. Temperature-programmed reaction spectroscopy

TPRS experiments were conducted using a fixed-bed microreactor connected to a quadrupole mass spectrometer (QMS) (Stanford Research Systems RGA 100) via a Balzers (TYP GEV 010) high-pressure gas inlet system. The QMS signals at mass-to-charge (m/e) ratios of 2(H_2), 4(He), 18(H_2O), 28(N_2 and CO), 30 (NO), 32(O_2), 44(CO_2 and N_2O), and 46(NO_2) were monitored during each experiment, and these were recorded together with the temperature by a PC. Before each run, a fresh sample (0.3 g) was loaded in a clean quartz reactor tube. The reactor tube was installed in a split tube furnace with a Type K thermocouple placed near the center of the reactor bed. The catalyst was reduced in flowing H_2 (40 mL/min) by heating from 30 to 300 (500) °C at 5 °C/min and soaking at 300 (500) °C for 1 h. The sample was then cooled in flowing He to 30 °C. A typical TPRS experiment was conducted by heating from 30 to 600 °C at 5 °C/min in flowing 1% NO/He (27 mL/min). The sample was soaked at 600 °C for 1 h to measure the steady-state NO decomposition activity. Subsequently, the sample was cooled to 30 °C in flowing 1% NO/He.

3. Results

Fig. 1 shows the normalized Pt L_3 XANES spectra of the Pt/SiO_2(1) catalyst after reduction in flowing H_2 at 300 °C, after subsequent exposure to 1% NO/He at 25 °C, and after heating in the reaction mixture to 300 °C. The L_3 XANES spectrum of a 25 μm Pt foil is shown for reference, and a

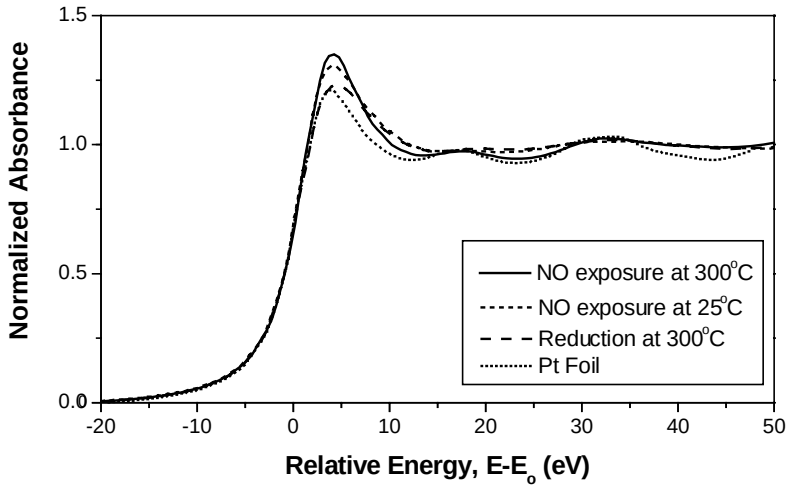

Fig. 1. Normalized Pt L_3 XANES spectra of Pt/SiO_2(1) after reduction in flowing H_2 at 300 °C, after subsequent exposure to 1% NO/He at 25 °C, and after heating in the reaction mixture to 300 °C. The L_3 XANES spectrum of a 25 μm Pt foil is shown for reference.

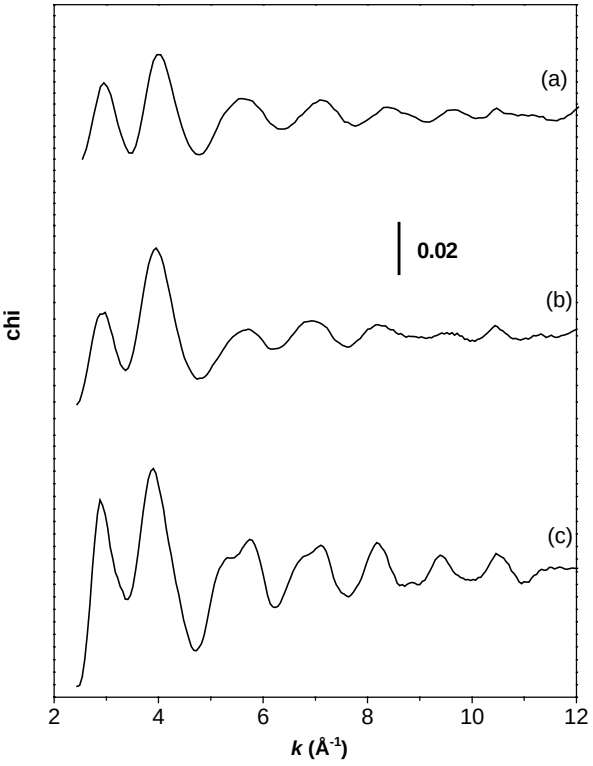

Fig. 2. Pt L_3 EXAFS spectra of $Pt/SiO_2(1)$ after reduction in flowing H_2 at 300 °C (a), after subsequent exposure to 1% NO/He at 25 °C (b), and after heating in the reaction mixture to 300 °C (c).

manual edge alignment has been performed in the −20 to 0 eV range. The Pt L_3 XANES spectrum is comprised of two components: the $2p^{3/2} \rightarrow 5d$ edge resonance (L_3 white line) and the continuum X-ray absorption threshold. The L_3 white line area is proportional to the density of unoccupied d states above the Fermi level and, hence, is sensitive to Pt oxidation state and chemical interactions with adsorbed species. The XANES spectrum of the $Pt/SiO_2(1)$ catalyst after reduction is closely similar to that of Pt foil from −20 to ∼4 eV; however, there are significant differences at higher energies. The L_3 white line is broadened and has additional area in the region between 5 and 15 eV. Moreover, the XAFS oscillations beginning at ∼10 eV are much weaker in the XANES spectrum of the $Pt/SiO_2(1)$ catalyst. The L_3 white line area of the catalyst increases significantly upon exposure to 1% NO/He at 25 °C; however, the XAFS is qualitatively similar to that of the reduced catalyst: the white line is broadened, and the XAFS oscillations are weak. In contrast, the XANES spectrum recorded after heating the catalyst in 1% NO/He at 300 °C for 30 min exhibits a sharper more distinct white line and larger XAFS oscillations.

The Pt L_3 EXAFS spectra of the $Pt/SiO_2(1)$ catalyst after the above-mentioned in situ treatments are shown in Fig. 2, and the corresponding k^3-weighted, Pt–Pt phase-corrected Fourier transforms are shown in Fig. 3. The EXAFS oscillations are very weak, especially at high k, for the reduced catalyst and the catalyst after NO exposure at 25 °C. The

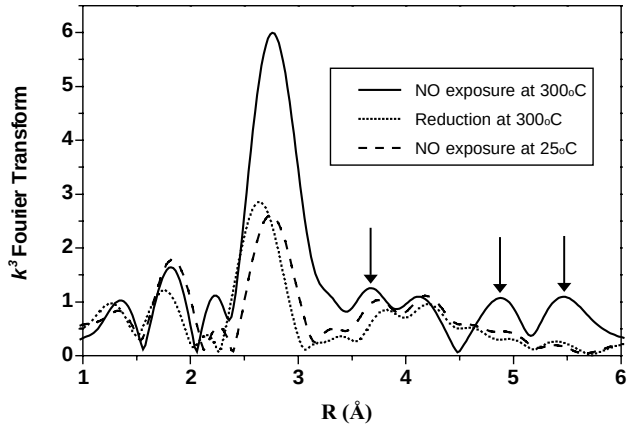

Fig. 3. Fourier transforms (k^3-weighted, Pt–Pt phase-corrected) of the EXAFS spectra of $Pt/SiO_2(1)$ after reduction in flowing H_2 at 300 °C, after subsequent exposure to 1% NO/He at 25 °C, and after heating in the reaction mixture to 300 °C.

amplitude of the high-k EXAFS oscillations increases significantly after heating the catalyst in 1% NO/He at 300 °C. Moreover, EXAFS oscillations due to backscattering from Pt higher shells are also evident. The FT EXAFS spectra of the reduced catalyst and the catalyst after NO exposure at 25 °C exhibit prominent first-shell Pt–Pt peaks at ∼2.65 and ∼2.75 Å, respectively. After heating the catalyst in 1% NO/He at 300 °C the first-shell Pt–Pt peak at ∼2.75 Å increases markedly in intensity and higher shell Pt–Pt contributions appear (as indicated by arrows). The results obtained by fitting the EXAFS spectra in the ranges of $2.8 < k < 11.5\ Å^{-1}$ and $1.0 < R < 3.0$ Å are given in Table 2.

Fig. 4 shows the normalized Pt L_3 XANES spectra of the $Pt/SiO_2(2)$, Pt/Al_2O_3, and Pt/MgO catalysts after reduction in flowing H_2 at 300 °C and after subsequent treatment in 1% NO/He at 300 °C (except for Pt/Al_2O_3). The L_3 XANES spectrum of the $Pt/SiO_2(2)$ catalyst after reduction (Fig. 4a) is very similar to that of Pt foil suggesting the presence of Pt crystallites. In contrast, the L_3 white line areas of the Pt/Al_2O_3 and Pt/MgO catalysts after reduction (Fig. 4b and c, respectively) are significantly larger than that of Pt foil indicating that the Pt was not completely reduced. The Pt/Al_2O_3 catalyst in particular contains a significant percentage of oxidized Pt, and for this reason we did not measure its XA spectrum after treatment in NO. An increase in

Table 2
EXAFS fitting results for $Pt/SiO_2(1)$ catalyst

Treatment	Shell	N	R (Å)	$\Delta\sigma^2$ (Å^2)	ΔE_0 (eV)
300 °C, H_2	Pt–Pt	5.8	2.66	0.0042	6.9
	Pt–O	0.5	2.01	0.013	0
25 °C, 1% NO/He	Pt–Pt	5.8	2.76	0.0051	1.6
	Pt–O/N	2.2	1.85	0.017	8.8
300 °C, 1% NO/He	Pt–Pt	8.6	2.76	0.0023	2.6

Typical errors in EXAFS parameters are ±15% for the coordination number, N, ±0.01 for the interatomic distance, R, and ±15% for the Debye–Waller factor, $\Delta\sigma^2$.

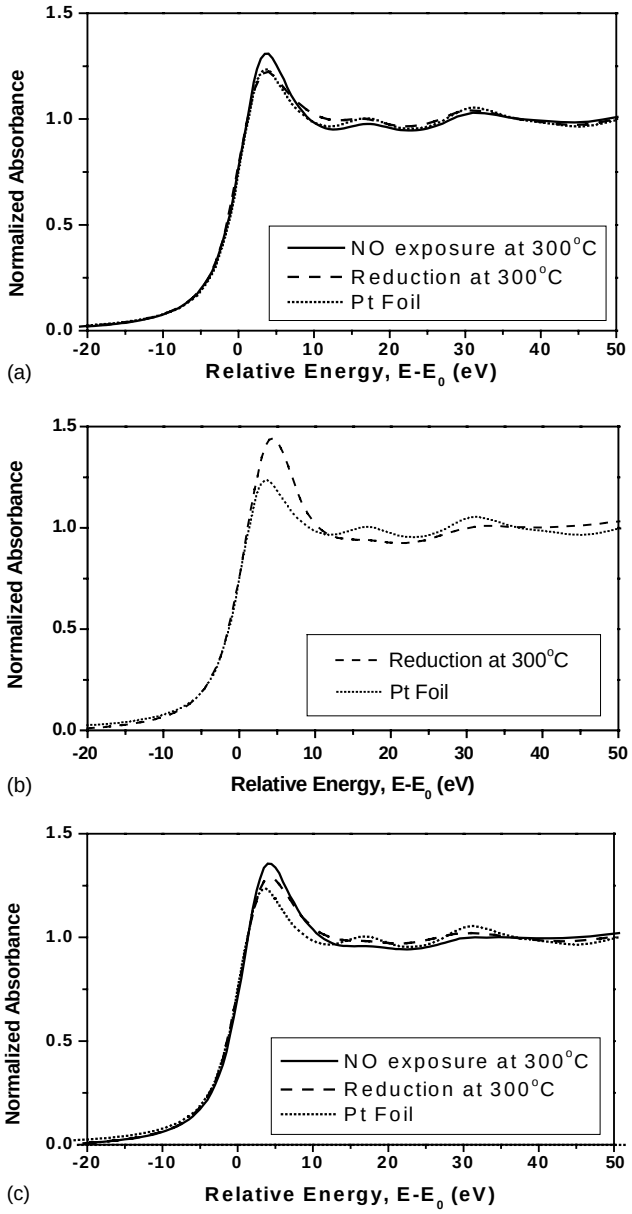

Fig. 4. Pt L_3 XANES spectra after reduction in flowing H_2 at 300 °C and after subsequent treatment in 1% NO/He at 300 °C: (a) $Pt/SiO_2(2)$, (b) Pt/Al_2O_3, and (c) Pt/MgO. The L_3 XANES spectrum of a 25 μm Pt foil is shown for reference.

white line area is observed for the $Pt/SiO_2(2)$ and Pt/MgO catalysts after heating in flowing 1% NO/He at 300 °C. The $Pt/SiO_2(2)$ catalyst exhibits a smaller increase in white line area after this NO treatment than the $Pt/SiO_2(1)$ catalyst. The Pt L_3 white line areas of the Pt/MgO and $Pt/SiO_2(1)$ catalysts are approximately equal after NO treatment at 300 °C.

The Pt L_3 EXAFS spectra of the $Pt/SiO_2(2)$, Pt/Al_2O_3, and Pt/MgO catalysts after reduction in H_2 at 300 °C are shown in Fig. 5. The amplitude of the high-k EXAFS oscillations is greater for the $Pt/SiO_2(2)$ catalyst; moreover, there are higher frequency contributions due to backscattering from second, third, and fourth nearest neighbor Pt atoms. The EXAFS

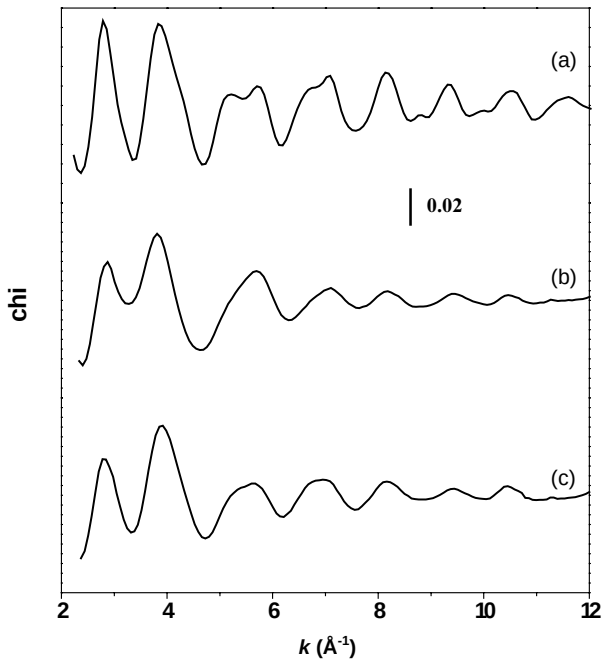

Fig. 5. Pt L_3 EXAFS spectrum of (a) $Pt/SiO_2(2)$, (b) Pt/Al_2O_3, and (c) Pt/MgO catalysts after reduction in flowing H_2 at 300 °C.

spectra of the Pt/Al_2O_3 and Pt/MgO catalysts contain first nearest neighbor contributions from Pt (major) and O (minor) backscatterers. The k^3-weighted, Pt–Pt phase-corrected Fourier transforms of the EXAFS spectra are shown in Fig. 6. The FT EXAFS spectrum of the $Pt/SiO_2(2)$ catalyst exhibits a prominent first-shell Pt–Pt peak at ∼2.75 Å and

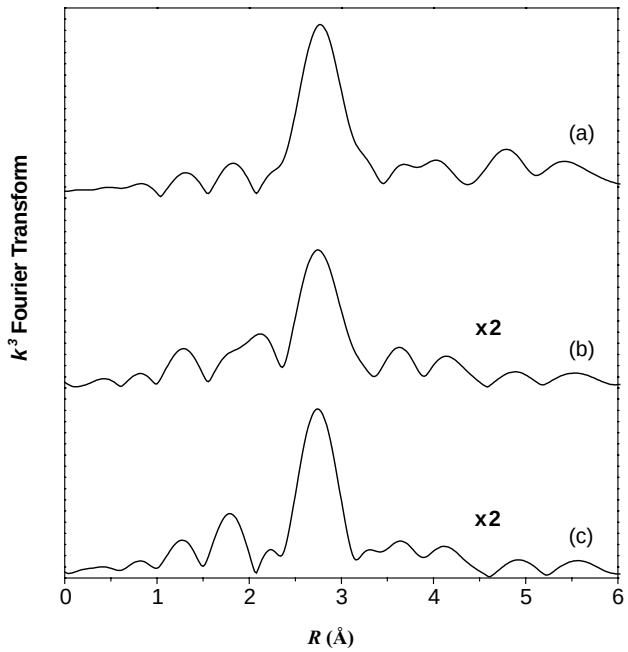

Fig. 6. Fourier transforms (k^3-weighted, Pt–Pt phase-corrected) of the EXAFS spectra of (a) $Pt/SiO_2(2)$, (b) Pt/Al_2O_3, and (c) Pt/MgO after reduction in flowing H_2 at 300 °C.

Table 3
EXAFS fitting results for supported Pt catalysts after reduction at 300 °C

Catalyst	Shell	N	R (Å)	$\Delta\sigma^2$ (Å^2)	ΔE_0 (eV)
Pt/SiO_2(2)	Pt–Pt	9.7	2.77	0.0009	3.7
Pt/Al_2O_3	Pt–Pt	6.1	2.75	0.0077	0.2
	Pt–O	2.2	2.02	0.0080	3.6
Pt/MgO	Pt–Pt	7.0	2.76	0.0071	1.5
	Pt–O	0.8	1.96	0.0087	0

Typical errors in EXAFS parameters are ±15% for the coordination number, N, ±0.01 for the interatomic distance, R, and ±15% for the Debye–Waller factor, $\Delta\sigma^2$.

higher shell Pt–Pt contributions consistent with the f.c.c. crystal structure. The first-shell Pt–Pt peaks for the Pt/Al_2O_3 and Pt/MgO catalysts are much weaker, and there are low-R features indicative of Pt–O backscattering (particularly for the Pt/Al_2O_3 catalyst). The results obtained by fitting the EXAFS spectra in the ranges of $2.8 < k < 11.5\,\text{Å}^{-1}$ and $1.0 < R < 3.0\,\text{Å}$ are given in Table 3.

The EXAFS spectra of the Pt/SiO_2(2) and Pt/MgO catalysts after heating to 300 °C in flowing 1% NO/He (not shown) are closely similar to those of the reduced catalysts (shown in Figs. 5 and 6) indicating that the supported Pt particles do not sinter under these conditions.

The temporal TPRS profiles for the Pt/SiO_2(1), Pt/SiO_2(2), Pt/Al_2O_3, and Pt/TiO_2 catalysts after in situ reduction at 300 °C are shown in Fig. 7. The temperature program, product (N_2, O_2, N_2O) and reactant (NO) QMS traces are displayed versus on-stream time. The switch from He to 1% NO/He flow results in the partial pressure transients observed within the first 100 s on stream. NO consumption and concomitant N_2O and N_2 evolution are observed between 150 and 250 °C over each supported Pt catalyst. The TPRS product profiles are plotted with respect to temperature in Fig. 8. The Pt/Al_2O_3 catalyst shows transient NO decomposition activity beginning at 150 °C—about 50 °C lower than the other catalysts. The Pt/SiO_2(2) and Pt/TiO_2 catalysts exhibit weak N_2O production maxima at approximately 250 °C. Direct decomposition of NO to N_2 and O_2, as evidenced by O_2 evolution, commences at approximately 350 °C over each catalyst. NO consumption increases progressively as the catalyst temperature is increased, and N_2O production diminishes markedly above 400 °C. For each catalyst, steady-state NO decomposition activity is achieved after ca. 1 h on stream at 600 °C. When the raw QMS signals are calibrated to account for the relative sensitivities of the detector and inlet system, the steady-state N_2:O_2 ratio is found to be very close to the expected 1:1 stoichiometry. The N_2O selectivity is negligible under steady-state reaction conditions at 600 °C. A sharp NO consumption peak and a small N_2 evolution peak are observed for the Pt/Al_2O_3 catalyst during rapid cooling in flowing 1% NO/He after NO decomposition catalysis.

Fig. 9 shows the temporal TPRS profiles for the Pt/MgO catalyst after reduction at 300 and 500 °C. A large NO consumption peak is observed at 250 °C for the catalyst reduced at 300 °C (Fig. 9a). The concomitant $m/e = 28$ and 44 gas evolution peaks are due primarily to CO and CO_2 (as evidenced by a strong $m/e = 12$ fragment). These TPRS features are virtually eliminated after reduction at 500 °C (Fig. 9b), and only modest amounts of N_2 and N_2O are produced at low temperature. Direct decomposition of NO to N_2

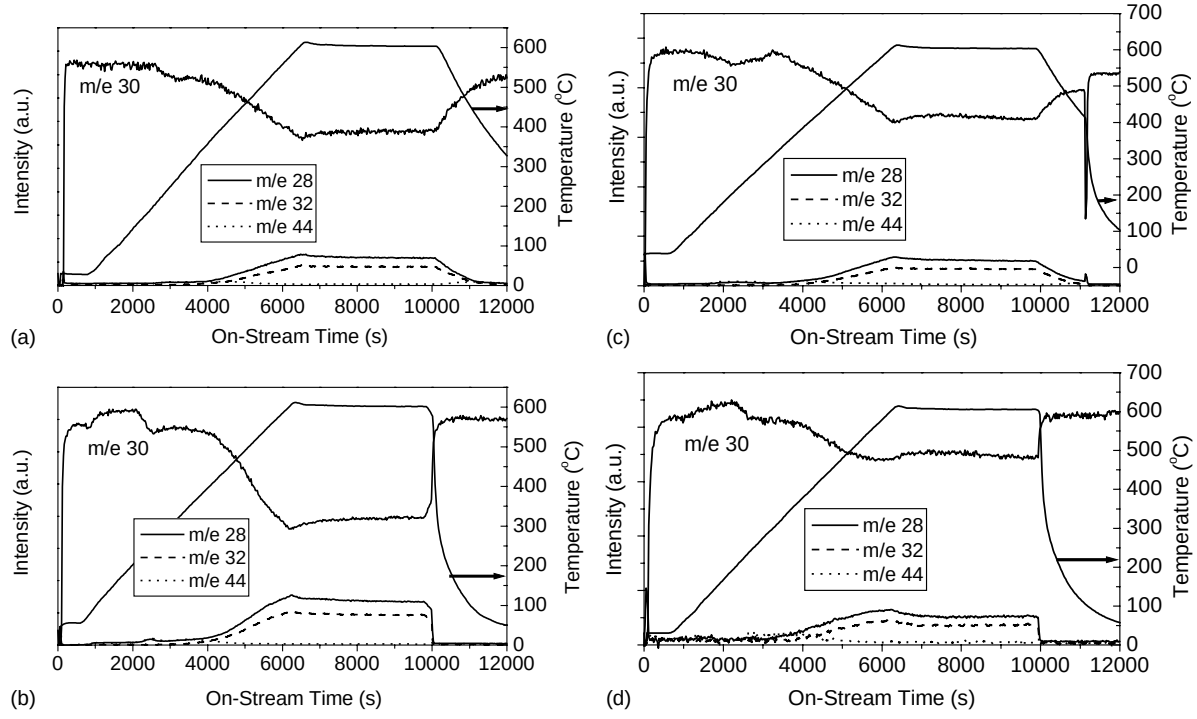

Fig. 7. 1% NO/He TPRS profiles of supported Pt catalysts (time abscissa): (a) Pt/SiO_2(1), (b) Pt/SiO_2(2), (c) Pt/Al_2O_3, and (d) Pt/TiO_2.

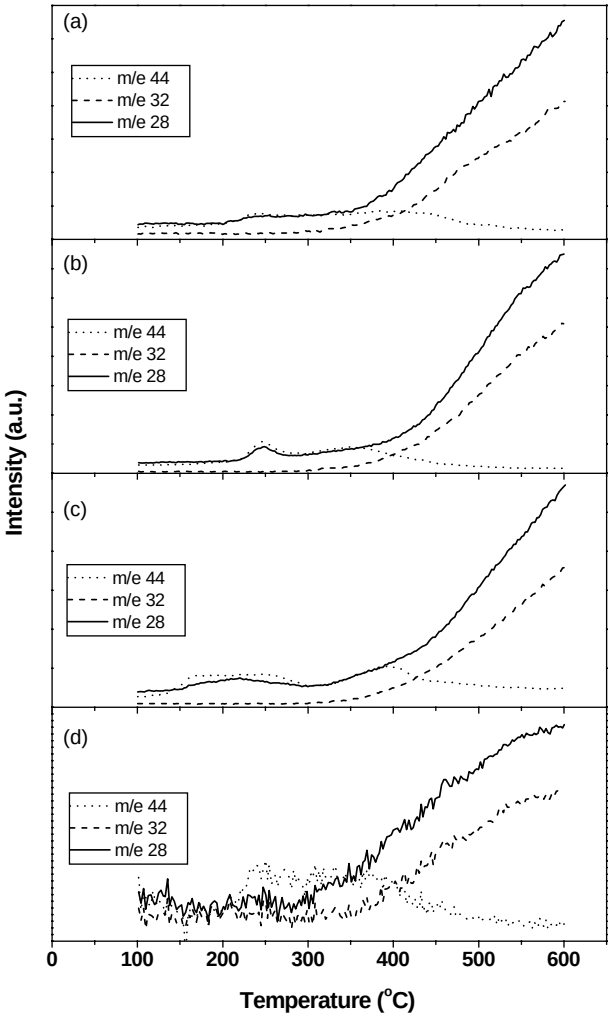

Fig. 8. 1% NO/He TPRS profiles of supported Pt catalysts (temperature abscissa): (a) $Pt/SiO_2(1)$, (b) $Pt/SiO_2(2)$, (c) Pt/Al_2O_3, and (d) Pt/TiO_2.

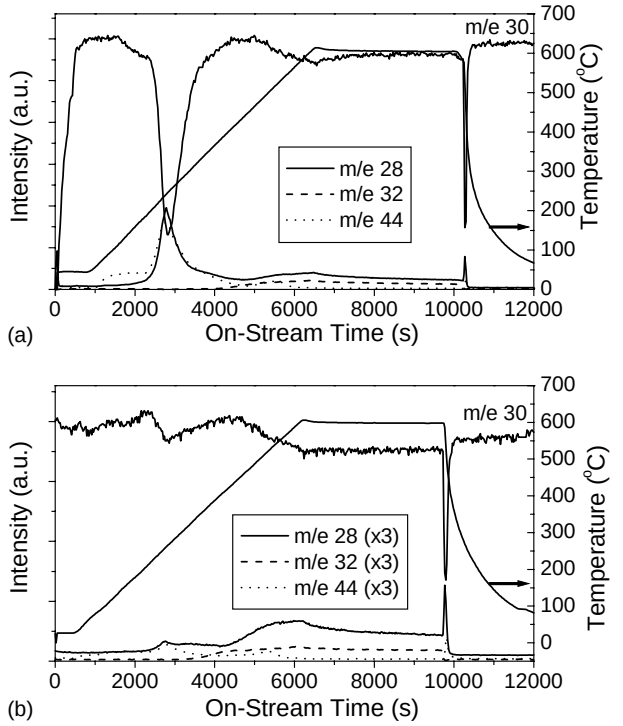

Fig. 9. 1% NO/He TPRS profiles (time abscissa) of Pt/MgO prepared using $[Pt(acac)_2]$ after reduction in flowing H_2 at (a) 300 °C and (b) 500 °C.

and O_2 (as evidenced by O_2 evolution) begins at 300–350 °C, and a unique N_2O evolution peak is observed at approximately 500 °C. Steady-state NO decomposition activity is observed at 600 °C; however, the catalytic activity is significantly lower than the other supported Pt catalysts. After NO decomposition catalysis, a sharp NO consumption peak accompanied by N_2 and N_2O evolution is observed during rapid cooling in flowing 1% NO/He.

The steady-state NO conversions measured at 600 °C for the supported Pt catalysts after reduction in H_2 at 300 °C are listed in Table 1. The measured conversions are not differential and, hence, cannot be used to determine reaction rates directly; however, NO decomposition over Pt is known to obey first-order kinetics with respect to NO [9–11]. The reaction rates given in Table 1 were calculated from the measured conversions by assuming plug flow behavior and first-order kinetics. The rates represent the steady-state activities of the catalysts extrapolated to 0% conversion for a 1% NO/He feed. This approach does not account for any rate inhibition due to O_2 produced by the reaction. On this basis, the steady-state NO decomposition activities of the catalysts after 300 °C reduction decrease in the order: $Pt/Al_2O_3 \approx Pt/SiO_2(1) > Pt/SiO_2(2) \approx Pt/TiO_2 > Pt/MgO$. The $Pt/SiO_2(2)$ and Pt/TiO_2 catalysts have equivalent activities; the $Pt/SiO_2(1)$ and Pt/Al_2O_3 catalysts are significantly more active; and the Pt/MgO catalyst is significantly less active. Additional NO decomposition activity measurements were made on selected catalysts after reduction at 500 °C, and these data are included in Table 1. The steady-state NO decomposition rates for the $Pt/SiO_2(2)$, Pt/Al_2O_3, and Pt/TiO_2 catalysts after 500 °C reduction are equivalent within experimental uncertainty. The primary effect of the higher reduction temperature is to reduce the activity of the Pt/Al_2O_3 catalyst bringing it in line with $Pt/SiO_2(2)$ and Pt/TiO_2. The NO decomposition activities of the latter catalysts are not changed by increasing the reduction temperature. The catalytic activity of Pt/MgO increases after reduction in H_2 at 500 °C, but it remains significantly less active than the other supported Pt catalysts.

4. Discussion

The $Pt/SiO_2(1)$ catalyst after reduction in H_2 at 300 °C contains small (∼1 nm) Pt clusters that exhibit a Pt–Pt nearest neighbor distance that is 0.09 Å shorter than in bulk Pt with a large relative Debye–Waller factor. Reifsnyder et al. [19] examined a similarly prepared Pt/SiO_2 catalyst by

in situ XAFS spectroscopy at liquid-nitrogen temperature and obtained high-quality EXAFS data that are fully consistent with the results presented herein. We infer that the short Pt–Pt distance and large disorder of the Pt–Pt shell are typical of silica-supported Pt clusters in the absence of chemisorbed hydrogen. Exposure of the supported Pt clusters to NO at 25 °C results in an increase in Pt L_3 white line area, relaxation of the Pt–Pt bond length, and the appearance of low-Z backscatterers in the EXAFS spectrum; however, the average Pt–Pt coordination number does not change, indicating that the clusters do not aggregate under these conditions. The low-Z backscatterers are N and/or O atoms at an average distance of 1.85 Å. The large Debye–Waller factor of this shell suggests a broad distribution of Pt–N/O distances arising from a mixture of molecularly adsorbed NO, N_{ads}, and O_{ads}. The increase in Pt L_3 white line area can be explained by electron transfer from the Pt 5d orbitals to the $2\pi^*$ orbital of molecularly adsorbed NO and/or by the presence of N_{ads} and O_{ads} species. For comparison, the Pt–N distance for a single bent nitrosyl ligand in a Pt_{19} carbonyl cluster is 1.80 Å [20], and density functional theory calculations for NO adsorbed on Pt(1 0 0) surfaces provide the following values: Pt–NO (linear atop), 1.82 Å; Pt_2–NO (bridge), 1.98 Å; Pt_2–N (bridge), 1.87 Å; and Pt_2–O (bridge), 1.96 Å [21]. We do not, however, observe significant backscattering from the nitrosyl O atom of adsorbed NO.

A large increase in the first-shell Pt–Pt coordination number and the appearance of Pt higher shells were observed after heating the Pt/SiO_2(1) catalyst in 1% NO/He at 300 °C for 30 min. These observations indicate that the original Pt clusters aggregate to form Pt crystallites under these conditions. Lööf et al. previously reported rapid sintering of ≤1 nm Pt particles on γ-Al_2O_3 upon exposure to dilute NO mixtures at temperatures as low as 200 °C, whereas the supported particles resisted sintering in Ar and H_2 at temperatures up to 700 °C [22]. Moreover, the loss of Pt dispersion (as measured by CO TPD and transmission electron microscopy) did not depend strongly on either temperature (above 300 °C) nor NO concentration (0.1–4% in Ar). An in situ EXAFS spectroscopy study by Schneider et al. yielded similar results for a pre-reduced 1.16 wt.% Pt/Al_2O_3 catalyst ($N_{Pt-Pt} = 7$) that was exposed to flowing 1% NO/N_2 at 300 °C [23]. A marked increase in the Pt–Pt coordination number and a concomitant decrease in the Debye–Waller factor were observed. Both groups invoke mobile Pt^{n+} nitrosyl species as possible intermediates in the rapid sintering of supported Pt particles in an NO ambient.

The EXAFS fitting results for the remaining catalysts (Table 3) indicate that the average Pt–Pt coordination number decreases in the sequence: $Pt/SiO_2(2) > Pt/MgO \approx Pt/Al_2O_3$. The low first-shell Debye–Waller factor and strong contributions from higher Pt–Pt shells indicate that the Pt/SiO_2(2) catalyst contains well-ordered Pt crystallites. The significant Pt–O contribution at 2.02 Å for the Pt/Al_2O_3 catalyst is indicative of Pt oxide species. Analysis of the EXAFS spectra (not shown) of the calcined Pt/SiO_2 and Pt/Al_2O_3 catalysts indicates that the Pt is in the form of a PtO_2-like species with a Pt–O coordination number of ∼6 and a Pt–O distance of 2.04 Å. By assuming that the oxidized Pt remains as Pt(IV) with an octahedral Pt–O coordination environment, we estimate that ∼1/3 of the Pt in the Pt/Al_2O_3 sample was not reduced at 300 °C. The average Pt oxidation state of +4/3 is consistent with the XANES spectrum of the Pt/Al_2O_3 catalyst. Correction of the average Pt–Pt coordination number of the Pt/Al_2O_3 catalyst to account for the oxidized Pt increases the Pt–Pt coordination number of the metal particles to ∼9. The EXAFS spectrum of the Pt/MgO catalyst contains a contribution from O backscatterers at 1.96 Å consistent with unreduced [$Pt(acac)_2$] species. Using a Pt–O coordination number of 4 for [$Pt(acac)_2$], we estimate that ∼20% of the Pt in the Pt/MgO sample was not reduced at 300 °C. Correction of the average Pt–Pt coordination number of the Pt/MgO catalyst also increases the Pt–Pt coordination number of the metal particles to ∼9. These estimated Pt–Pt coordination numbers represent approximate lower bounds for the fully reduced Pt/Al_2O_3 and Pt/MgO catalysts (e.g., after 500 °C reduction). In contrast to the nanometer-sized Pt clusters in the reduced Pt/SiO_2(1) catalyst, the larger supported Pt particles in the Pt/SiO_2(2) and Pt/MgO catalysts resist sintering under flowing 1% NO/He at 300 °C.

Our TPRS results are in good agreement with previous research on direct NO decomposition over supported Pt [3,5,8–10]. The data evidence that at low temperatures (less than 400 °C) NO is decomposed to produce N_2O and N_2. For the Pt/SiO_2 and Pt/Al_2O_3 catalysts, the low-temperature N_2O and N_2 traces are nearly coincident leading us to suggest that these species are produced by parallel surface reactions. The following sequence of elementary surface steps can account for N_2O and N_2 formation at low temperatures [4,24]:

$$NO \rightarrow NO_{ads} \quad (1)$$

$$NO_{ads} \rightarrow N_{ads} + O_{ads} \quad (2)$$

$$NO_{ads} + N_{ads} \rightarrow N_2O \quad (3)$$

$$NO_{ads} + N_{ads} \rightarrow N_2 + O_{ads} \quad (4)$$

Molecular (Eq. (1)) and dissociative (Eq. (2)) chemisorption of NO on Pt are competitive processes at 200–400 °C, and we suggest that reaction between molecularly adsorbed NO and adsorbed N atoms results in N_2O and N_2 production (Eqs. (3) and (4), respectively). These low-temperature NO decomposition reactions result in net accumulation of oxygen on the catalyst. The increased Pt L_3 white line intensities after heating in 1% NO/He at 300 °C evidence oxidation of the supported Pt particles consistent with oxygen poisoning [3,6]. As the catalyst temperature is increased, the N_2O selectivity decreases, the N_2 selectivity increases, and O_2 production commences at approximately 350 °C. The onset of O_2 production corresponds closely to the TPD peak temperatures reported for O_2 desorption from Pt/Al_2O_3 catalysts

[8] and from the Pt (1 0 0) − (5 × 20) surface after ≥0.5 langmuirs exposure to NO at 100 K [13]. The N_2O selectivity approaches zero at 500 °C, and above this temperature only N_2 and O_2 are produced. We infer that these products are formed by associative desorption of N and O atoms:

$$2N_{ads} \rightarrow N_2 \quad (5)$$

$$2O_{ads} \rightarrow O_2 \quad (6)$$

The N_2:O_2 stoichiometry is essentially 1:1 for steady-state NO decomposition at 600 °C, and catalyst deactivation is insignificant on the time scale of our experiments.

$Pt/SiO_2(1)$ is significantly more active for NO decomposition than $Pt/SiO_2(2)$ after 300 °C reduction, and the smaller Pt–Pt coordination number of $Pt/SiO_2(1)$ after heating in 1% NO/He at 300 °C is indicative of a higher Pt dispersion (D). In order to compare the intrinsic activities of the Pt/SiO_2 catalysts, TOFs were estimated from the steady-state NO decomposition rates at 600 °C for a 1% NO/He feed. Pt dispersions were estimated from the first-shell Pt–Pt coordination numbers using the following empirical formula [25]:

$$D = 2.0 - 0.167N \quad (7)$$

An equivalent expression can be obtained by modeling the supported Pt particles as cubo-octahedra, relating N to particle diameter d_p (nm), and approximating D as d_p^{-1}. The resulting TOFs (Table 1) for the two Pt/SiO_2 catalysts are nearly equal [0.010 s^{-1} (±20%)] indicating that particle size effects are insignificant for direct NO decomposition over Pt/SiO_2 catalysts. The TOFs are in reasonably good agreement with those reported by Furusawa and Aika for NO decomposition over Pt/Al_2O_3 when corrected for their NO feed concentration of 0.1% NO/He [8]. These researchers found almost no variation in TOF with particle size for Pt/Al_2O_3 catalysts with Pt dispersions between 0.1 and 0.9 (as measured by H_2 chemisorption on freshly reduced samples). A modestly larger TOF was reported for supported Pt crystallites ∼150 nm in diameter. The absence of significant particle-size effects for direct NO decomposition is somewhat surprising given the structure sensitivity of NO dissociation on Pt single crystal surfaces [4]. One possible explanation is that NO dissociation and O_2 desorption are both kinetically significant steps in direct NO decomposition, and NO dissociation is more efficient on small Pt particles with a higher density of edge and corner sites, whereas O_2 desorption is more facile on larger Pt crystallites with a higher percentage of (1 1 1)-type facets [8].

The higher activity of the Pt/Al_2O_3 catalyst after reduction at 300 °C may be due to the presence of partially oxidized Pt species. Recent work by Schießer et al. indicates that partially oxidized Pt species are active sites for NO reduction by propane and propene over Pt/MCM-41 (Al_2O_3) [26]. Reduction temperature did not affect the NO decomposition performance of the $Pt/SiO_2(2)$ and Pt/TiO_2 catalysts. In contrast, the reduction temperature of the Pt/MgO catalyst had a dramatic influence on its TPRS profile. After 300 °C reduction, organic residues from the [$Pt(acac)_2$] precursor remain on the catalyst surface and participate in NO reduction at ∼250 °C. The temperature-programmed reduction data for Pt/MgO supports this conclusion; large quantities of CH_4 are produced between 300 and 500 °C. After pretreatment of Pt/MgO in flowing H_2 at 500 °C, the large NO consumption feature at ∼250 °C is virtually eliminated. An explanation for the increased NO decomposition activity of the Pt/MgO catalyst after 500 °C reduction will require additional data.

The equivalent NO decomposition activities of the $Pt/SiO_2(2)$, Pt/Al_2O_3, and Pt/TiO_2 catalysts after 500 °C reduction suggest the absence of significant support effects for Pt on these metal oxides. The lower NO decomposition activity of the Pt/MgO catalyst may be related to the strong basicity of the alkaline-earth metal oxide support. There is recent evidence that the oxidation resistance of supported Pt is greater on more acidic supports, and conversely, lower on basic supports, such as MgO. Yazawa et al. employed Pt L_3 XANES to measure the average oxidation state of supported Pt catalysts after O_2 treatment at 550 °C [27]. A strong correlation was observed between the L_3 white line area and the Hammett acidity of the support, indicating greater oxidation of Pt supported on more basic metal oxides. A possible explanation for this behavior is that increasing metal oxide basicity decreases the Pt ionization potential due to a Coulombic interaction with support oxygen anions [28].

The sharp NO consumption feature seen during rapid cooling of the Pt/Al_2O_3 and Pt/MgO catalysts after NO decomposition catalysis (Figs. 7c and 9, respectively) results from a combination of NO decomposition and NO_x storage. Significantly, this phenomenon was only observed for Pt supported on more basic metal oxides. Some of the NO adsorbed during rapid cooling is decomposed to N_2 and N_2O; however, the product peaks are too small to account for the total NO uptake, indicating that an additional NO consumption mechanism is operative. Temperature-programmed desorption spectra (not shown) evidence that NO_x is stored on the support as surface nitrites and nitrates during cooling of the Pt/Al_2O_3 and Pt/MgO catalysts in 1% NO/He.

5. Conclusions

Low-temperature NO decomposition to N_2O and N_2 over supported Pt catalysts results in oxidation of the Pt particles consistent with oxygen poisoning. Small (∼1 nm) Pt clusters on SiO_2 sinter during heating in 1% NO/He at 300 °C. The TOF for direct NO decomposition over Pt/SiO_2 catalysts at 600 °C is insensitive to Pt particle size. The $Pt/SiO_2(2)$, Pt/Al_2O_3, and Pt/TiO_2 catalysts (after reduction at 500 °C) have equivalent NO decomposition activities suggesting the absence of support effects. In contrast, the NO decomposition activity of Pt supported on strongly basic MgO is significantly lower. Transient NO consumption observed during rapid cooling of the Pt/Al_2O_3 and Pt/MgO catalysts in 1%

NO/He (after steady-state catalysis at 600°C) is attributed to NO decomposition and NO_x storage on the support.

Acknowledgements

This research was sponsored by Caterpillar, Inc. and the US Department of Energy. The XAS experiments were performed using beam line X-11A of the National Synchrotron Light Source at Brookhaven National Laboratory. The authors wish to thank Bryan Silletti of Caterpillar for his contributions to this work.

References

[1] A. Fritz, V. Pitchon, Appl. Catal. B 13 (1997) 1.
[2] C.T. Goralski Jr., W.F. Schneider, Appl. Catal. B 37 (2002) 263.
[3] J.W. Hightower, D.A. Van Leirsburg, in: R.L. Kimilish, J.G. Larson (Eds.), The Catalytic Chemistry of Nitrogen Oxides, Plenum Press, New York, 1975, p. 63.
[4] F. Garin, Appl. Catal. A 222 (2001) 183.
[5] A. Gervasini, P. Carniti, V. Ragaini, Appl. Catal. B 22 (1999) 201.
[6] R. Burch, T.C. Watling, Catal. Lett. 37 (1996) 51.
[7] R.J. Wu, T.Y. Chou, C.T. Yeh, Appl. Catal. B 6 (1995) 105.
[8] T. Furusawa, K. Aika, Bull. Chem. Soc. Jpn. 73 (2000) 795.
[9] A. Amirnazmi, J.E. Benson, M. Boudart, J. Catal. 30 (1973) 55.
[10] A. Amirnazmi, M. Boudart, J. Catal. 39 (1975) 383.
[11] M.J. Mummey, L.D. Schmidt, Surf. Sci. 109 (1981) 29.
[12] R.J. Gorte, L.D. Schmidt, J.L. Gland, Surf. Sci. 109 (1981) 367.
[13] C. Panja, B.E. Koel, J. Phys. Chem. A 104 (2000) 2486.
[14] M. Che, C.O. Bennett, Adv. Catal. 36 (1989) 55.
[15] D.R. Rainer, S.M. Vesecky, M. Koranne, W.S. Oh, D.W. Goodman, J. Catal. 167 (1997) 234.
[16] K. Sakata, T. Uchijima, Y. Yoneda, Nippon Kagaku Kaishi 6 (1978) 791.
[17] F.W.H. Kampers, T.M.J. Maas, J. Van Grondelle, P. Brinkgreve, D.C. Koningsberger, Rev. Sci. Instrum. 60 (1989) 2635.
[18] M. Vaarkamp, J.C. Linders, D.C. Koningsberger, Physica B 208/209 (1995) 159.
[19] S.N. Reifsnyder, M.M. Otten, D.E. Sayers, H.H. Lamb, J. Phys. Chem. B 101 (1997) 4972.
[20] A. Ceriotti, N. Masciocchi, P. Macchi, G. Longoni, Angew Chem. Int. Ed. 38 (1999) 3724.
[21] Q. Ge, M. Neurock, J. Am. Chem. Soc. 126 (2004) 1551.
[22] P. Lööf, B. Stenbom, H. Nordén, B. Kasemo, J. Catal. 144 (1993) 60.
[23] S. Schneider, D. Bazin, F. Garin, G. Maire, M. Capelle, G. Meunier, R. Noirot, Appl. Catal. A 189 (1999) 139.
[24] W.A. Brown, D.A. King, J. Phys. Chem. B 104 (2000) 2578.
[25] B.J. Kip, F.B.M. Duivenvoorden, D.C. Koningsberger, R. Prins, J. Catal. 105 (1987) 26.
[26] W. Schießer, H. Vinek, A. Jentys, Catal. Lett. 73 (2001) 67.
[27] Y. Yazawa, N. Takagi, H. Yoshida, S. Komai, A. Satsuma, T. Tanaka, S. Yoshida, T. Hattori, Appl. Catal. A 233 (2002) 103.
[28] B.L. Mojet, J.T. Miller, D.E. Ramaker, D.C. Koningsberger, J. Catal. 186 (1999) 373.